Arithmetic of focused vortex beams in three-dimensional optical lattice arrays

Jeffrey A. Davis,[1] Don M. Cottrell,[1] Kyle R. McCormick,[1] Jorge Albero,[2] and Ignacio Moreno[3,*]

[1]Department of Physics, San Diego State University, San Diego, California 92182-1233, USA

[2]Département Micro Nano Sciences et Systèmes, Institut FEMTO-ST (UMR CNRS 6174), Université de Franche-Comté, 25030 Besançon cedex, France

[3]Departamento de Ciencia de Materiales, Óptica y Tecnología Electrónica, Universidad Miguel Hernández, 03202 Elche, Spain

*Corresponding author: i.moreno@umh.es

Received 13 December 2013; revised 7 February 2014; accepted 14 February 2014; posted 18 February 2014 (Doc. ID 202897); published 25 March 2014

In this work, we present a method to generate a 3D lattice of vortex beams. We apply phase look-up tables (LUTs) designed to generate gratings having an arbitrary content of diffraction orders. This phase LUT can be applied to a variety of diffraction optical elements, such as linear phase gratings, blazed diffractive lenses, and spiral phase patterns. We concentrate on combinations of all of these to create 3D structures of vortex beams. In particular, we generate all of these elements in the first output quadrant and eliminate the zero-order diffraction that often unavoidably accompanies these patterns. We discuss different ways of producing these 3D vortex gratings, and how the various output beams are related to the arithmetic of the 3D distribution of topological charges. Experimental results are provided by means of a liquid crystal spatial light modulator.

OCIS codes: (050.1950) Diffraction gratings; (050.1965) Diffractive lenses; (050.4865) Optical vortices; (070.6120) Spatial light modulators.

http://dx.doi.org/10.1364/AO.53.002040

1. Introduction

Recently there has been a great deal of interest in producing 3D arrays of focused spots of light. These light structures are of interest to create 3D lattice structures, such as photonic crystal structures with photosensitized media [1], 3D optical tweezers [2], 3D optical manipulation [3], or 3D probing of biomedical systems [4]. Such structures can be generated with sequential direct laser writing to produce an array of focus spots [5], or alternatively with parallel processing approaches. Multiple beam interference [6] and diffractive optical elements [7,8] have been demonstrated to provide such parallel production. Some approaches include multiplexing Fresnel lenses to allow focalization in multiple planes [9]. The use of spatial light modulators (SLMs) additionally adds the flexibility to sequentially program holograms and diffractive elements [10]. Although higher quality optical elements can be made using micro-optic techniques [8], this comes with a loss in the programmability provided with SLMs.

One important issue is to produce focus spots with equal intensity. In two dimensions, this has been traditionally accomplished with the classical Dammann grating [11] or with continuous phase fan-out elements [12]. The Dammann grating is a specially designed binary phase (0, π) grating that creates a number of diffracted orders with equal intensity in a plane. We recently extended this Dammann grating to produce a 3D lattice of focus spots with equal intensity and demonstrated it with a phase-only

1559-128X/14/102040-11$15.00/0

SLM [13]. This was obtained by applying the same transition points of the standard Dammann grating to more general phase profiles, which included linear but also quadratic phase profiles to achieve multiple focalizations within a plane and multiple planes of focalization. More recently, the same concept has been applied a with higher spatial resolution diffractive mask to be applied in systems with high numerical aperture (NA) [14].

In parallel, the generation of vortex beams is of interest in a variety of applications. This is typically created by means of a spiral phase plate. The number q of 2π steps along the azimuthal coordinate determines the topological charge of the created vortex beam. Sometimes the spiral phase plate can be embedded onto a diffraction grating, creating a forked grating [15], or onto a diffractive lens, creating a spiral lens [16].

Some works combine these two previous ideas and extend the schemes to create a 3D array of focused vortex beams. This can be done by multiplying the spiral phase by a grating designed to create multiple focalizations [17,18], thus replicating the vortex beam on the location of each focused spot. In this work, we will define this as a global spiral phase because it is applied identically to each of the diffracted orders. Another option is to divide the diffractive screen onto different areas where different vortex creating elements are encoded [19]. This option allows the encoding of different topological charges onto different locations, but introduces losses in available space bandwidth.

Alternatively, different vortex beams can be obtained at different harmonic orders of a continuous phase diffractive element. This is done by applying a given nonlinear phase look-up table (LUT) to a designed first-order blazed diffractive element. In initial work, designs based on the above-mentioned binary phase Dammann gratings were produced to give a number of equally intense but different vortex charged diffraction orders [20]. We applied this type of design to a diffractive lens with an embedded spiral phase pattern in order to generate a number of equally intense vortex beams with different topological charges focused on different planes. The same concept was later applied to generate vortex 3D arrays in high NA systems [21], where a number of focus planes were obtained, each one showing a 2D array of vortex beams, all with the same charge within the plane, but changing from one plane to another.

However, there is a more versatile approach (other than Dammann gratings) for controlling the harmonic components of a diffractive phase element based on generalized continuous phase grating designs. We applied phase profiles based on the optimal design of laser beam splitters presented by Romero and Dickey [22,23]. These designs provide better diffraction efficiency than binary phase designs of Dammann gratings, and allow different intensity and phase control on different diffraction orders, as well as producing arbitrary target diffraction orders [24,25].

We report here on the generation of 3D arrays of focused vortex spots of light, using 3D grating splitter structures that combine regular 2D diffraction gratings to produce a number of focal spots in a plane, with diffractive lenses producing a number of focal planes. However, the output of such diffractive elements critically depends on the order in which the various structures are submitted to the phase LUT process, and this can result in very different vortex topological charge distributions on different focused planes and on different orders within a plane. The purpose of this work is to clearly state all these various options and determine the topological charges that are created in each case.

The approach is extremely simple to implement since it involves using suitably designed phase LUT functions for designing the beam splitter gratings. In addition, this system employs a single phase-only SLM where a single phase mask is addressed to produce the 3D structure, as opposed to other approaches that require more sophisticated optical architectures [21].

There is another critical element to this work. In many two and three grating designs, there is a strong DC order due to encoding errors, or to limitations of the SLM phase modulation. In addition, there are symmetry elements between output spots created in positive and negative orders. For this work, we decided to concentrate on designs where all of the output spots occur in the first quadrant, i.e., in the top right area with respect to the zero order, which defines the optical axis.

The paper is organized as follows: Section 2 briefly reviews the technique for optimal beam splitting with phase-only gratings [22,23]. Section 3 presents the application of the grating design to create vortex generating diffraction gratings. In particular we examine a number of different possibilities for generating different vortex charges in the various diffracted orders and concentrate on 1D and 2D examples to demonstrate the algebraic combinations. Then, in Section 4, we combine these cases to produce 3D vortex generating diffraction gratings, and again some examples of the different combinations are analyzed. All cases are illustrated with experimental results. Finally, we present the conclusions of the work.

2. Theory of Optimal Beam Splitting

Our approach requires the generation of an initial phase-only diffraction grating that has the flexibility to control which diffraction orders are present, their amplitudes, and their relative phases. This will yield a phase LUT that can then be applied to a number of phase optical elements, namely, blazed gratings and diffractive lenses. Although this topic has received some attention, it is important to review it because it is of pivotal importance to this work.

The optimal beam splitting design [22,23] consists of determining a one-dimensional continuous

phase-only function $\varphi(x)$ that will generate a desired number of diffracted orders having desired phase and amplitude values and written as

$$\exp[i\varphi(x)] = \frac{f(x)}{|f(x)|}, \tag{1}$$

where

$$f(x) = \sum_l \mu_l \exp[i\alpha_l] \exp[ilx]. \tag{2}$$

Here l is the integer index of each of the N target orders, and α_l and μ_l are the sets of numerical parameters that represent the phase and amplitude of each harmonic component, respectively.

In our previous work, we have explored the use of the SOLVER routine in Microsoft Excel, which employs a generalized reduced gradient algorithm [26] to determine the phase-only mapping (or phase LUT) that must be applied to a linear phase blazed grating profile to transform it onto the optimal phase profile $\varphi(x)$. This is done by computing the discrete set of numerical parameters α_l and μ_l in Eq. (2) that will produce the desired set of orders, their relative phases, and their strengths. The SOLVER routine acts as a multidimensional least square fit where we minimize the difference between the grating output produced by the discrete set of parameters in Eq. (2) and the desired output. As we have shown in previous work, we can produce a number of equally intense orders [20], with tailored intensity [24], and grating profiles where different orders can be selectively eliminated or enhanced. Some examples of these parameters were shown in [24]. Once these parameters have been determined, we can generate a phase mapping LUT. This LUT phase mapping can then be applied to produce generalized optimal gratings.

Consequently, we have demonstrated complete optimization of a desired grating structure to control the number, intensity, and phase of various diffracted orders. Moreover, as mentioned before, the grating phase profile can be applied to a variety of different diffractive optical element problems.

In this work, as stated earlier, we want to generate a grating that produces only the +1 and +2 diffracted orders with equal intensities. As a result, the coefficients given by the SOLVER routine are $\mu_1 = \mu_2 = 1$ and $\alpha_1 = \alpha_2 = 0$. Note that this particular case corresponds to a blazed grating with a phase range of 3π rad [27]. Using these parameters, we can form a phase LUT as shown in Fig. 1(a), which is the modulo 2π version of the above-mentioned blazed grating with 3π phase modulation. Here the horizontal axis gives the initial phase values for a linear phase-only grating that would produce only a single +1 diffracted order. The vertical axis shows how these phase values would be mapped to produce a desired grating. Figure 1(b) shows the initial phase profile for a 1D blazed grating, while Fig. 1(c) shows the result of this phase mapping provided by the LUT in Fig. 1(a). Three periods of the grating are shown in each case. Note that both gratings show the same periodicity, but the phase profile has been modified in Fig. 1(c) to create the duplicator. This new grating would then produce only the +1 and +2 diffracted orders, as shown previously in Fig. 1 of Ref. [25].

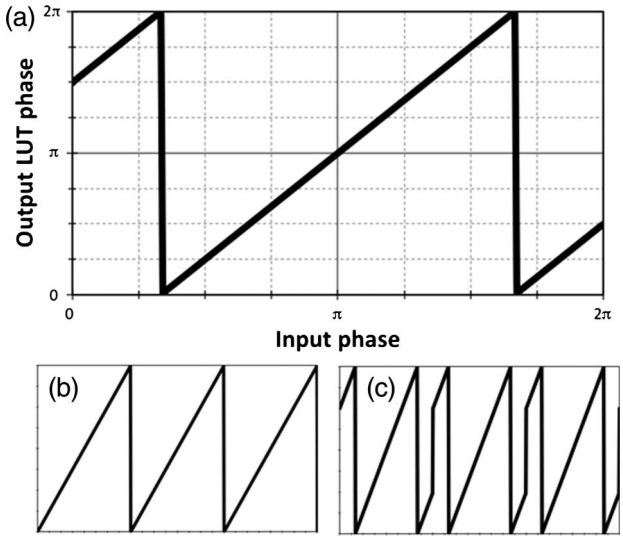

Fig. 1. (a) Phase LUT_{12} to produce equally intense +1 and +2 orders. (b) Initial linear phase grating (three periods are shown). (c) Phase grating resulting from the application of LUT_{12} to the linear phase grating.

This process will be further explored in Section 3.

3. Setup and Experimental Results

Before discussing the various grating types, we provide a discussion of the experimental setup. In that way, we can combine the theoretical discussions of the grating types with experimental proof in order to make the manuscript more readable. Because the notation for the 3D case will become quite complicated, we include here also some cases related to 1D and 2D diffraction gratings that illustrate the method later applied to the 3D gratings.

The calculated phase profiles have been experimentally tested with a transmissive parallel-aligned liquid crystal (LC) SLM manufactured by Seiko-Epson, with 640 × 480 pixels and pixel spacing of $\Delta = 42$ μm [28]. The SLM is illuminated with an argon ion laser operating at 514 nm, producing a phase-only response with more than 2π rad modulation depth. The beam is expanded with a spatial filter, collimated with a lens, and linearly polarized parallel to the LC director axis. After passing through the SLM, the beam is focused by a glass lens ($f = 39$ cm). The lens is located approximately 25 cm apart from the SLM (using a preexisting experimental setup). In later experiments, we will combine the glass lens with a lens written onto the SLM. By separating the two lenses, we were able to control the focal planes more accurately. Finally, a 20× objective lens is used to image the back focal plane of the glass lens onto a Wincam CCD camera.

A. Design of 1D Focusing of Vortex Gratings

We begin with a discussion of a 1D vortex-producing grating consisting of three terms as

$$t(x,y) = \exp(iq_G\theta) \cdot [\exp(iq_X\theta) \cdot \exp(i\gamma x)]. \quad (3)$$

Here, the last term is a linear phase as γx, where $\gamma = 2\pi/d$ and d is the period of the grating. The other two terms are spiral phases defined as $q\theta$, where q denotes the corresponding topological charge, and θ is the azimuthal coordinate. The first term is a global spiral phase $q_G\theta$ that will affect the remaining part of the grating. The second term is another spiral phase term $q_X\theta$ that is included in the x grating. This grating will create a single diffraction order with a vortex beam with topological charge $q_G + q_X$. We distinguish between the global spiral phase term (with charge q_G) and the spiral phase multiplying the linear grating (with charge q_X). While the first one will be added to the final modified grating, thus replicating an additional topological charge q_G to the complete array of vortex beams, the second one will be launched onto the phase LUT together with the linear grating, thus suffering the same kind of transformation and, therefore, producing different topological charges on different harmonic components.

Next we apply the technique of Eqs. (1) and (2) to the product of the second and third terms in Eq. (3). Our previous works [24,25] showed that this technique allows the generation of an arbitrary number of orders with arbitrary amplitudes and phases. However, for simplicity, we assume here a case study where the optimal phase profile of Eq. (2) is designed to produce only the first and second orders with equal energy as in Fig. 1. Consequently, the phase transmission function can be written as

$$\begin{aligned} t(x,y) &= \exp(iq_G\theta) \cdot \mathbf{LUT}_{12}[\exp(iq_X\theta) \cdot \exp(i\gamma x)] \\ &= \exp(iq_G\theta) \cdot \left[\sum_{l=1,2} c_l \exp(ilq_X\theta)\exp(il\gamma x)\right], \end{aligned} \quad (4)$$

where $\mathbf{LUT}_{12}$ denotes the phase transformation creating $+1$ and $+2$ diffraction orders with equal intensity, l is an integer number denoting the diffraction order, and c_l are the related coefficients of the Fourier expansion of the modified phase grating. The maximum efficiency that this $(+1, +2)$ duplicator can create is $|c_1|^2 = |c_2|^2 = 40.5\%$ [25]. The rest of the energy is distributed in other diffraction orders, which, for simplicity, have been ignored in the summary in Eq. (4).

Note that both the linear and the spiral phase terms within the square bracket in Eq. (4) are affected by the order l of the harmonic term in the Fourier expansion. Therefore, the diffraction order l will have a vortex beam with topological charge:

$$q_l = q_G + lq_X. \quad (5)$$

The Fourier transform of the grating in Eq. (4) will create now two diffracted orders consisting of vortices at locations $p = \gamma$ and $p = 2\gamma$. The charge of the first diffracted order will be $q_1 = q_G + q_X$, while the charge of the second diffracted order will be $q_2 = q_G + 2q_X$. So we have three variables—the global charge (q_G), the number of orders produced by the theory of Eq. (2), and the charge integrated into the linear grating (q_X). This illustrates the main aspect in the design of the vortex grating: while multiplying the spiral phase by a grating adds the global charge q_G to all generated orders, launching the spiral phase together with the linear phase to the phase LUT adds a topological charge $q_l = lq_X$ at each harmonic order l.

Figure 2 illustrates the appearance of some of these phase patterns and extends the treatment of Fig. 1. Figure 2(a) shows the linear phase grating, while Fig. 2(b) shows the result after applying the look-up table LUT_{12} from Fig. 1 to the linear phase. Note that the phase, here and in the rest of the cases,

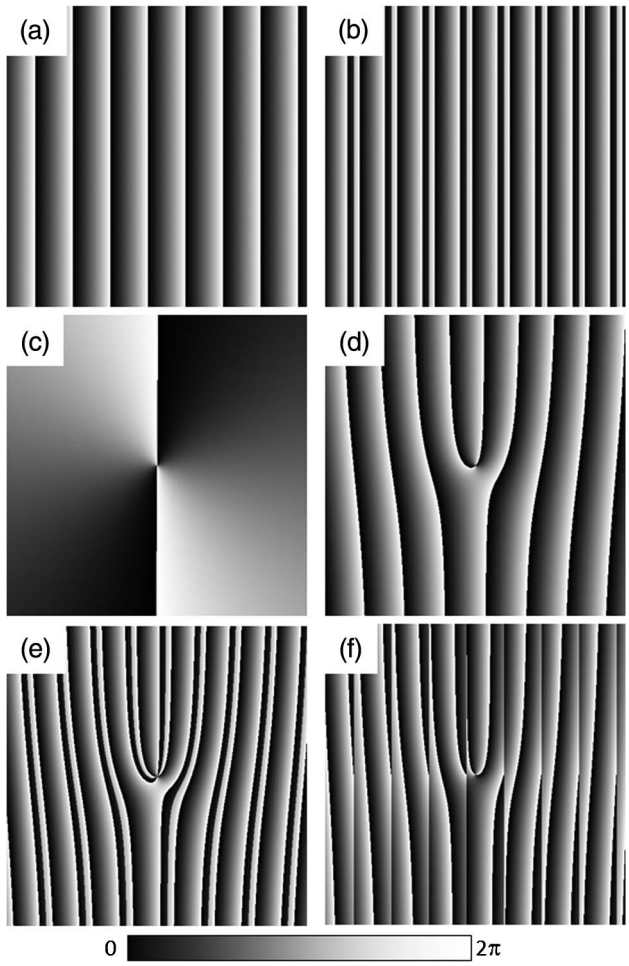

Fig. 2. Phase gratings design: (a) linear phase, (b) phase after LUT_{12} is applied to the linear phase in (a) to create the $(+1, +2)$ duplicator, (c) spiral phase ($q = 2$), (d) addition of the linear phase in (a) and the spiral phase in (c), (e) phase after LUT_{12} is applied to the phase grating in (d), and (f) addition of the $(+1, +2)$ duplicator grating in (b) with the spiral phase in (c).

is always presented as the modulo 2π version of the addition of the different phase elements. This modified grating shows the same periodicity as the linear phase grating, but the phases have been modified in order to create the duplicator grating on diffraction orders (+1, +2). Figure 2(c) shows the spiral phase pattern ($q = 2$) and it can be implemented in several ways. In the first case, Fig. 2(d) shows the addition of the linear phase from Fig. 2(a) with the spiral phase pattern from Fig. 2(c) to create the characteristic "fork" grating. This grating will produce a single diffraction order with the encoded vortex with topological charge $q = 2$.

However, we could obtain other different fork gratings. For instance, we could apply LUT_{12} from Fig. 1 to the linear phase grating in Fig. 2(d) and obtain the grating pattern shown in Fig. 2(e). This grating now would produce a first order having a charge of $q = 2$ and a second order having a charge of $q = 4$. Finally, we could alternatively add the spiral phase of Fig. 2(c) to the duplicator grating pattern from Fig. 2(b) to obtain the more complicated grating in Fig. 2(f). In this case, the added spiral phase acts as a global spiral pattern where $q_G = 2$. Now this grating would produce a first order and a second order both having a charge of $q = 2$.

Figure 3 shows the experimental output produced by our basic 1D design and is similar to results in [20]. Figure 3(a) shows the DC order, obtained when no grating is displayed on the SLM. Figure 3(b) shows the result with the grating designed to create only the $l = +1$ and $l = +2$ diffracted orders, i.e., the grating shown in Fig. 2(b). The output is mostly confined to these two positive orders, and the DC, negative orders, and higher positive orders are very weak. Next, Figs. 3(c) and 3(d) show the cases when the spiral phase is launched to the phase LUT together with the linear phase, with charges $q_x = +1$ and $q_x = +2$, respectively, [this last corresponds to Fig. 2(e)]. Note that now, according to Eq. (5), the

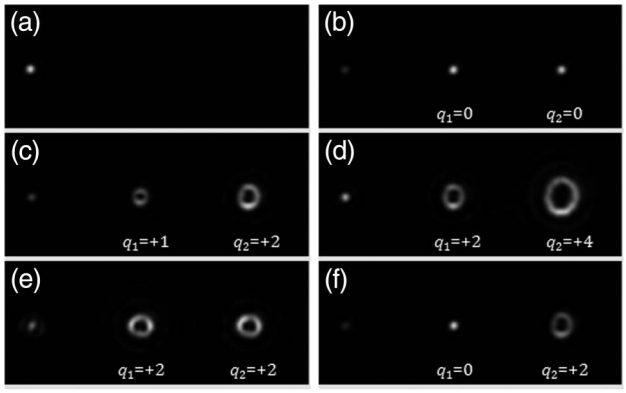

Fig. 3. Experimental diffraction patterns generated with 1D optimal phase gratings: (a) DC order (no grating is displayed), (b) (+1, +2) duplicator grating with equal intensity [mask in Fig. 2(b)], (c) grating with $q_X = +1$, (d) grating with $q_X = +2$ [mask in Fig. 2(e)], (e) grating with $q_G = 2$ [mask in Fig. 2(f)], and (f) grating with $q_G = -2$ $q_X = +2$. The generated charge q_{l_X} is indicated at each diffraction order l_X.

two diffraction orders carry vortex beams with different topological charges, where the charge at order $l = +2$ is twice the charge at order $l = +1$, as the bigger diameter shows in each case. The resulting topological charge is indicated with labels in each order.

In contrast, Fig. 3(e) shows the case when a global spiral phase term with a topological charge $q_G = +2$ is added to the previous optimal (+1, +2) duplicator, i.e., it corresponds to the grating in Fig. 2(f). In this case, the same vortex beam is replicated on both diffraction orders, and the two orders show the same diameter. Finally, Fig. 3(f) shows the case that combines $q_x = +2$ and a global charge $q_G = -2$. Note that now the total topological charge at the diffraction order $l = +1$ is $q_1 = q_G + q_x = 0$, yielding a bright spot. Here the global spiral term compensates for the spiral phase encoded onto the optimal grating. In contrast, at diffraction order $l = +2$, the total topological charge is $q_2 = q_G + 2q_x = +2$.

B. Design of 2D Focusing of Vortex Gratings

Next we consider the 2D version of this grating. Again for simplicity, we assume that the grating produces only the first and second orders. Consequently, the starting 2D phase transmission function similar to Eq. (3) will be written as

$$t(x,y) = \exp(iq_G\theta)\cdot[\exp(iq_X\theta)\cdot\exp(i\gamma_X x)] \cdot[\exp(iq_Y\theta)\cdot\exp(i\gamma_Y y)], \tag{6}$$

where now different linear phases $\gamma_X x$ and $\gamma_Y y$ and different charges q_X and q_Y can be encoded on each of the x and y directions. The phase-only grating in Eq. (6) will produce a single diffraction order at location $(p_X, p_Y) = (\gamma_X, \gamma_Y)$ with topological charge $q = q_G + q_X + q_Y$. However, when a phase LUT is applied to the different components, additional vortex charges can be obtained at different harmonic components.

We apply the technique of Eqs. (1) and (2) twice to the phase pattern in Eq. (6): first to the product of the second and third terms (first square brackets) and then for the product of the fourth and fifth terms (second square brackets). Again, for simplicity, we assume that the optimal phase profile of Eq. (2) produces only the first and second orders, and the periods are selected equal in the x and y directions. Consequently, the phase transmission function is written as

$$\begin{aligned} t(x,y) &= e^{iq_G\theta}\mathbf{LUT}_{12}[e^{iq_X\theta}e^{i\gamma_X x}]\cdot\mathbf{LUT}_{12}[e^{iq_Y\theta}e^{i\gamma_Y y}] \\ &= e^{iq_G\theta}\left[\sum_{l_x=1,2} c_{l_X} e^{il_X q_X\theta} e^{il_X\gamma_X x}\right] \\ &\quad\cdot\left[\sum_{l_y=1,2} c_{l_Y} e^{il_Y q_Y\theta} e^{il_Y\gamma_Y y}\right]. \end{aligned} \tag{7}$$

The Fourier transform of this grating will create four diffracted orders at locations $(p_X, p_Y) = (l_X\gamma_X, l_Y\gamma_Y)$. Here l_X and l_Y are integer numbers denoting these harmonic orders in the x and y directions, respectively. The topological charge at each order will be given by $q_{l_X l_Y} = q_G + l_X q_X + l_Y q_Y$. For instance, the first diffracted order ($l_X = l_Y = +1$) at the location $(p_X, p_Y) = (\gamma_X, \gamma_Y)$ will have a total topological charge of $q_{11} = q_G + q_X + q_Y$. Another diffracted order will be formed at the location $(p_X, p_Y) = (2\gamma_X, \gamma_Y)$ with charge of $q_{21} = q_G + 2q_X + q_Y$, and another at the location $(p_X, p_Y) = (\gamma_X, 2\gamma_Y)$ with charge $q_{12} = q_G + q_X + 2q_Y$. Finally, the fourth diffracted order will be located at $(p_X, p_Y) = (2\gamma_X, 2\gamma_Y)$ and will have a charge of $q_{22} = q_G + 2q_X + 2q_Y$. So now we have four variables—the global charge (q_G), the number of diffraction orders produced for each grating, and the charges q_X and q_Y integrated into the two linear gratings.

Figure 4 illustrates the appearance of some of the phase gratings in this case. Figure 4(a) shows the case when two (+1, +2) duplicators are combined, one oriented in the x direction [like the one in Fig. 2(a)] and the second one in the y direction, in order to create a 2D distribution of diffraction orders. Now the phase mask shows a 2D interference pattern. Figure 4(b) illustrates the phase mask when this previous 2D mask is combined with a global spiral phase ($q_G = +2$) in Fig. 2(a). The phase pattern is rather similar, but note the "fork" interference shape that is present now in the center of the grating.

Related experimental results are presented in Fig. 5. Figure 5(a) shows again the DC order in the lower left corner for reference. Figure 5(b) shows the result when (+1, +2) duplicators in the x and y directions are multiplied [i.e., this case corresponds to the mask in Fig. 4(a)]. The resulting grating creates the 2×2 array of equally intense diffraction orders within a plane. Note that we selected the same period in the x and y directions ($\gamma_X = \gamma_Y$). In Fig. 5(c) a global spiral phase with topological charge $q_G = +2$ is added [i.e., this case corresponds to the mask in Fig. 4(b)]. Now the diffraction pattern shows the convolution of the delta functions in Fig. 5(b) with the vortex beam, which is, therefore, replicated in all four orders. Note that the diameter of the circle of light is the same in all four orders.

Other cases are shown in Figs. 5(d)–5(f) where no global spiral phase is added ($q_G = 0$), but spiral phases are incorporated onto the grating before the optimal phase LUT is applied. For instance, in Fig. 5(d) a topological charge $q_X = +2$ is added in the x direction (while leaving $q_Y = 0$). Now the vortex

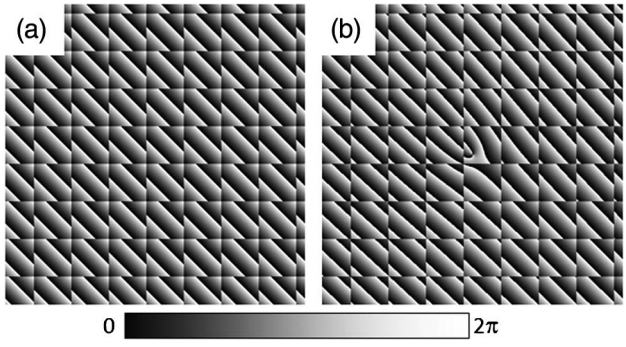

Fig. 4. Design of optical lattice arrays: (a) addition of the (+1, +2) duplicator grating in Fig. 1(c) with a 90 deg rotated version of itself to create a 2D array and (b) addition of this previous phase with the spiral phase in Fig. 2(c).

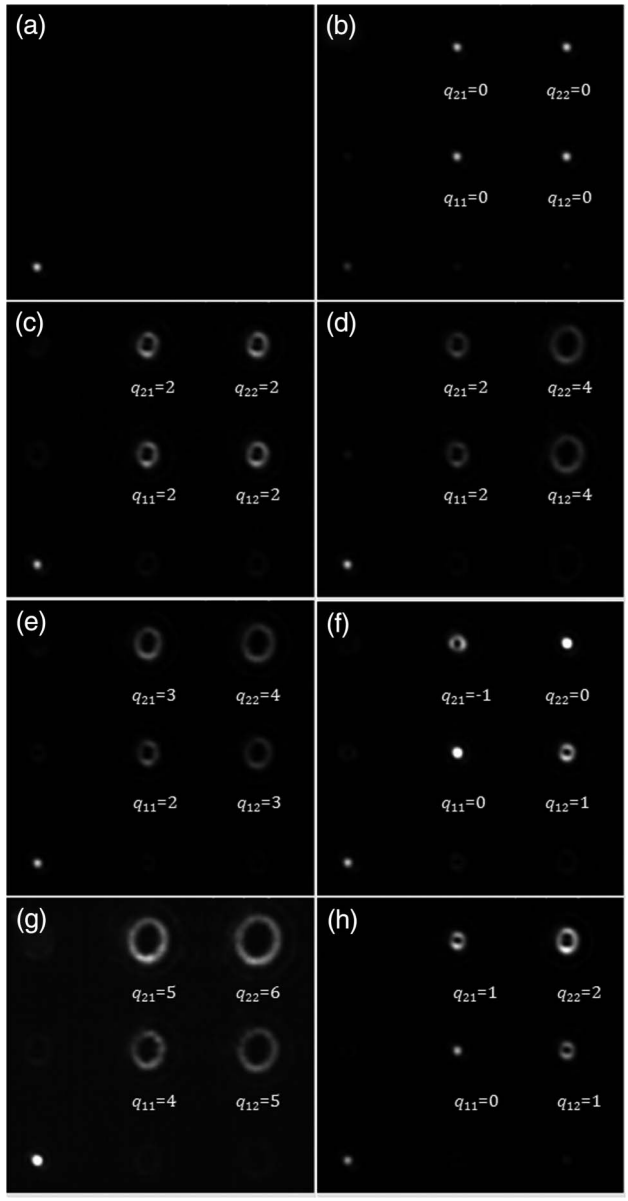

Fig. 5. Experimental diffraction patterns generated with 2D optimal phase gratings: (a) DC order (no grating is displayed), (b) $(+1, +2) \times (+1, +2)$ grating with equal intensity [mask in Fig. 4(a)], (c) grating with $q_G = +2$ [mask in Fig. 4(b)], (d) grating with $q_X = +2$, (e) grating with $q_X = q_Y = +1$, (f) grating with $q_X = +1$ and $q_Y = -1$, (g) grating with $q_G = +2$ and $q_X = q_Y = +1$, and (h) grating with $q_G = -2$ and $q_X = q_Y = +1$. The generated charge $q_{l_X l_Y}$ is indicated at each diffraction order (l_X, l_Y).

beam generated on the two orders with $l_X = +1$ show the same topological change $q_{11} = q_{12} = q_X = +2$, while the other two orders show vortices with $q_{21} = q_{22} = 2q_X = +4$, as shown by the larger diameter. Note the difference with the results in Fig. 5(e). Here the encoded spiral phase patterns have $q_X = +1$ and $q_Y = +1$. Therefore, again, four vortex beams are generated. The topological charges at orders ($l_X = +1$, $l_Y = +1$) and ($l_X = +2$, $l_Y = +2$) are $q_{11} = q_X + q_Y = +2$ and $q_{22} = 2q_X + 2q_Y = +4$, respectively. Although the total charge in these orders is identical to that in Fig. 5(d), there is a different contribution from the x and y components. This is clearer in the other two orders. The same topological charge $q_{12} = q_X + 2q_Y = +3$ and $q_{21} = 2q_X + q_Y = +3$ is obtained at orders ($l_X = +1$, $l_Y = +2$) and ($l_X = +2$, $l_Y = +1$), respectively. The charge (diameter) of the circle of light in these two orders is between that of the other two generated orders.

Another interesting case is shown in Fig. 5(f). Now charges $q_X = +1$ and $q_Y = -1$ are encoded onto the gratings launched onto the phase LUT. Therefore, vortex beams are generated at orders ($l_X = +1$, $l_Y = +2$) and ($l_X = +2$, $l_Y = +1$) with charges $q_{12} = q_X + 2q_Y = -1$ and $q_{21} = 2q_x + q_y = +1$, respectively. These vortex beams show the smallest diameter. Note that the sign difference is not detected in this experiment since vortex beams with charge $\pm q$ provide the same diameter on the focused order. The detection of the sign would require another vortex grating detector, as proposed in [29]. On the contrary, diagonal diffraction orders ($l_X = +1$, $l_Y = +1$) and ($l_X = +2$, $l_Y = +2$) show no vortex content since $q_{11} = q_X + q_Y = 0$ and $q_{22} = 2q_X + 2q_Y = 0$.

Finally, in Figs. 5(g) and 5(h) we added a global spiral phase. In both cases, charges $q_X = q_Y = +1$ are selected, i.e., the same case as in Fig. 5(e). However, now we add different global charges $q_G = +2$ in Fig. 5(g) and $q_G = -2$ in Fig. 5(h). Therefore, the global charge q_G is added in each of the four diffraction orders. In Fig. 5(g) we now obtain larger charges (bigger diameters) since the charges are $q_{11} = q_G + q_X + q_Y = +4$, $q_{21} = q_G + 2q_X + q_Y = +5$, $q_{12} = q_G + q_X + 2q_Y = +5$, and $q_{22} = q_G + 2q_X + 2q_Y = +6$. In contrast, and because of the negative sign in q_G, the results in Fig. 2(h) show smaller charges $q_{11} = q_G + q_X + q_Y = 0$, $q_{21} = q_G + 2q_X + q_Y = +1$, $q_{12} = q_G + q_X + 2q_Y = +1$, and $q_{22} = q_G + 2q_X + 2q_Y = +2$.

These results show the multiple alternatives that can be applied to create different 2D vortex beam array structures within a plane.

4. Design of 3D Focusing of Vortex Grating

Finally, this section describes the extension of the method to create the 3D gratings. To add the third dimension, we multiply the 2D case of Eq. (7) by a focusing lens function with its own charge (i.e., a vortex producing lens, as in [30]). The result is a transmission function as

$$t(x,y,z) = \exp(iq_G\theta)\cdot[\exp(iq_X\theta)\cdot\exp(i\gamma_X x)]\cdot[\exp(iq_Y\theta)\cdot\exp(i\gamma_Y y)]\cdot\left[\exp(iq_Z\theta)\cdot\exp\left(i\frac{\pi r^2}{\lambda f}\right)\right]. \quad (8)$$

Here, the quadratic phase term $\pi r^2/\lambda f$ is added, where $r = \sqrt{x^2 + y^2}$ is the radial coordinate and f denotes the selected focal length. A related additional spiral phase term with topological charge q_Z is also added.

This phase-only grating will produce a single diffraction order at location $(p_X, p_Y) = (\gamma_X, \gamma_Y)$, at a focal plane a distance f from the SLM, with a total topological charge $q = q_G + q_X + q_Y + q_Z$. However, again, when a phase LUT is applied to the different components, an additional vortex array structure can be obtained.

Thus, next we apply the technique of Eqs. (1) and (2) three times—first to the product of the second and third terms [first square brackets in Eq. (8)], then for the product of the fourth and fifth terms (second square brackets), and finally for the product of the lens function with its spiral charge (third square brackets). Again, for simplicity, we assume that the optimal phase profile of Eq. (2) produces only the first and second orders. Consequently, the phase transmission function is written as

$$t(x,y,z) = e^{iq_G\theta}\cdot\left[\sum_{l_X=1,2} c_{l_X} e^{il_X q_X\theta} e^{il_X\gamma_X x}\right]\cdot\left[\sum_{l_Y=1,2} c_{l_Y} e^{il_Y q_Y\theta} e^{il_Y\gamma_Y y}\right]\cdot\left[\sum_{l_Z=1,2} c_{l_Z} e^{il_Z q_Z\theta} e^{il_Z\frac{\pi r^2}{\lambda f}}\right]. \quad (9)$$

Here l_X, l_Y, and l_Z are integer numbers denoting the harmonic orders in the x, y, and z directions, respectively.

The resulting phase masks are illustrated in Figs. 6(a) and 6(b). Figure 6(a) shows how the

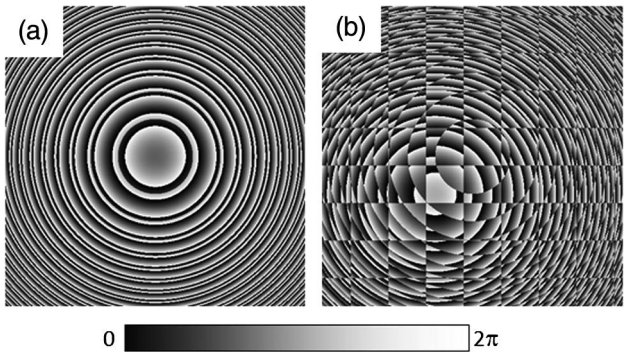

Fig. 6. Design of optical lens arrays: (a) the phase after LUT_{12} is applied to a quadratic lens phase and (b) addition of the phase grating in Fig. 4(a) and the lens phase in (a) to create a 3D focusing array.

quadratic phase factor of a lens is modified by the LUT_{12} in Fig. 1(a). Note how the same phase profile as in the linear grating in Fig. 1(c) is now radially distributed, following the quadratic period profile characteristic of a lens. We note that the raised harmonic components for the quadratic phase terms correspond to multiple quadratic phases with focal lengths defined by focal lengths f/l_Z. Therefore, this grating will create two focal planes at distances of f and $f/2$.

Figure 6(b) illustrates the grating resulting from combining the lens profile in Fig. 6(a) and the 2D phase grating in Fig. 4(a). Now, this phase mask will produce again two focal planes, and each one will have four diffracted orders, as in the 2D case. Therefore, a 3D structure is created, and different vortex values can be added onto the different dimensions (X, Y or Z). In addition to the 2D vortex structure created in each plane, an additional topological charge is given by the charge q_Z encoded on the lens function. Therefore, we denote the charge at each generated (l_X, l_Y, l_Z) diffraction order as $q_{l_X l_Y l_Z}$ and it will be given by $q_{l_X l_Y l_Z} = q_G + l_X q_X + l_Y q_Y + l_Z q_Z$.

First we discuss the first focal plane at $l_Z = 1$. The first diffracted order at the location $(p_X, p_Y) = (\gamma_X, \gamma_Y)$ will have a charge of $q_{111} = q_G + q_X + q_Y + q_Z$. Another diffracted order will be formed at the location $(p_X, p_Y) = (2\gamma_X, \gamma_Y)$ with charge $q_{211} = q_G + 2q_X + q_Y + q_Z$. The third diffracted order located at $(p_X, p_Y) = (\gamma_X, 2\gamma_Y)$ will have a charge of $q_{121} = q_G + q_X + 2q_Y + q_Z$. Finally the fourth diffracted order will be located at $(p_X, p_Y) = (2\gamma_X, 2\gamma_Y)$ and will have a charge of $q_{221} = q_G + 2q_X + 2q_Y + q_Z$. In contrast, at the second focal plane at $l_Z = 2$, the charges at the same locations, $(p_X, p_Y) = (\gamma_X, \gamma_Y)$, $(p_X, p_Y) = (\gamma_X, 2\gamma_Y)$, $(p_X, p_Y) = (2\gamma_X, \gamma_Y)$, and $(p_X, p_Y) = (2\gamma_X, 2\gamma_Y)$, will be, respectively, $q_{112} = q_G + q_X + q_Y + 2q_Z$, $q_{212} = q_G + 2q_X + q_Y + 2q_Z$, $q_{122} = q_G + q_X + 2q_Y + 2q_Z$, and $q_{222} = q_G + 2q_X + 2q_Y + 2q_Z$.

So now we have seven variables—the global charge (q_G), the number of orders produced by the theory of Eq. (2) for each grating, the charges integrated into the two linear gratings (q_X and q_Y), the number of focalizations produced again by the theory in Eq. (2), and the charge (q_Z) encoded into the lens grating.

Note that all the charges can have positive, negative, or even fractional values. Hence each diffracted order will consist of the sum of the various charge elements. This is the basis for this paper's title, which indicates we are investigating vortex arithmetic.

To make things even more general, we note that we can apply the phase LUT to any combination of the components in Eq. (8). For example, we could form the product of the x and y gratings, and then apply the LUT. In addition, we have complete freedom in choosing the number of orders that each LUT will generate, as well as their relative strengths and phases. Again, we concentrate here only on the case where the LUT generates two orders for simplicity.

Figures 7 and 8 show the final set of experiments, where we also included quadratic phase terms to create additional focal planes. In all cases, the final mask is designed to provide two focal planes resulting from harmonic components $l_Z = 1$ and $l_Z = 2$ from a quadratic phase term with a selected focal length for a diverging lens where $f = -4000$ mm. This value is large enough to avoid sampling effects.

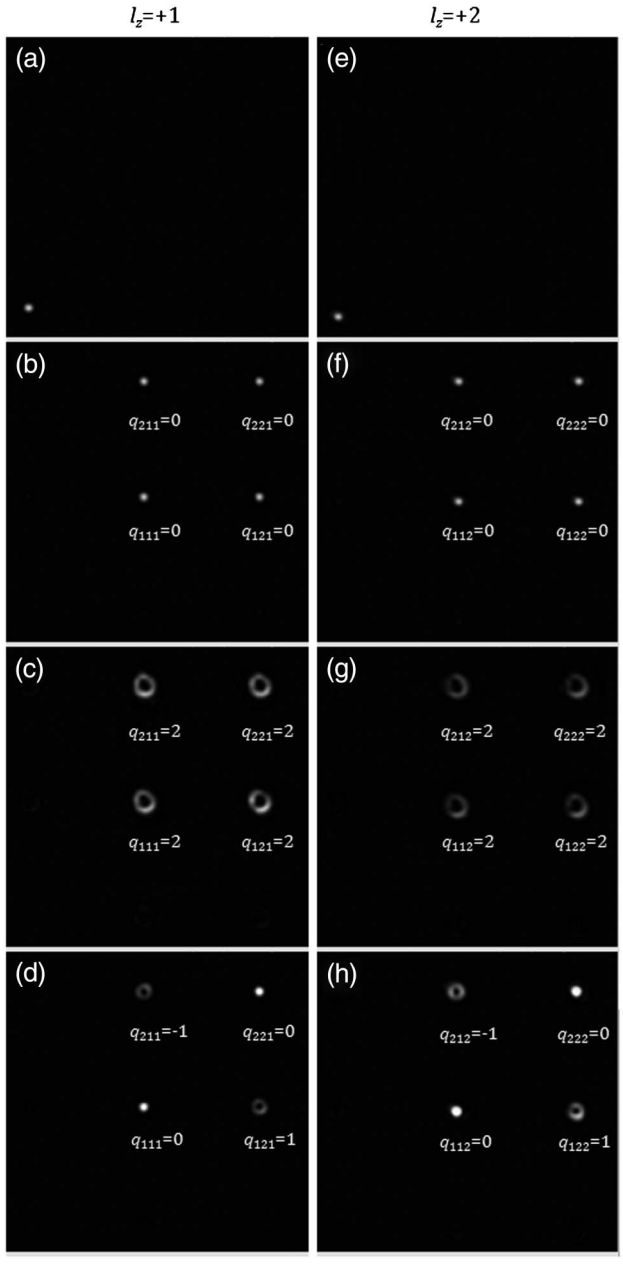

Fig. 7. Experimental diffraction patterns generated with 3D optimal phase gratings. Left and right columns show images at axial planes $l_Z = +1$ and $l_Z = +2$, respectively: (a) and (e) (+1, +2) lens [mask in Fig. 6(a)], (b) and (f) (+1, +2) lens multiplied by grating with four equal intensity orders [mask in Fig. 6(b)], (c) and (g) (+1, +2) lens multiplied by grating with $q_G = +2$, and (d) and (h) (+1, +2) lens multiplied by grating with $q_X = +1$ and $q_Y = -1$. The generated charge q_{l_X, l_Y, l_Z} is indicated at each diffraction order (l_X, l_Y, l_Z).

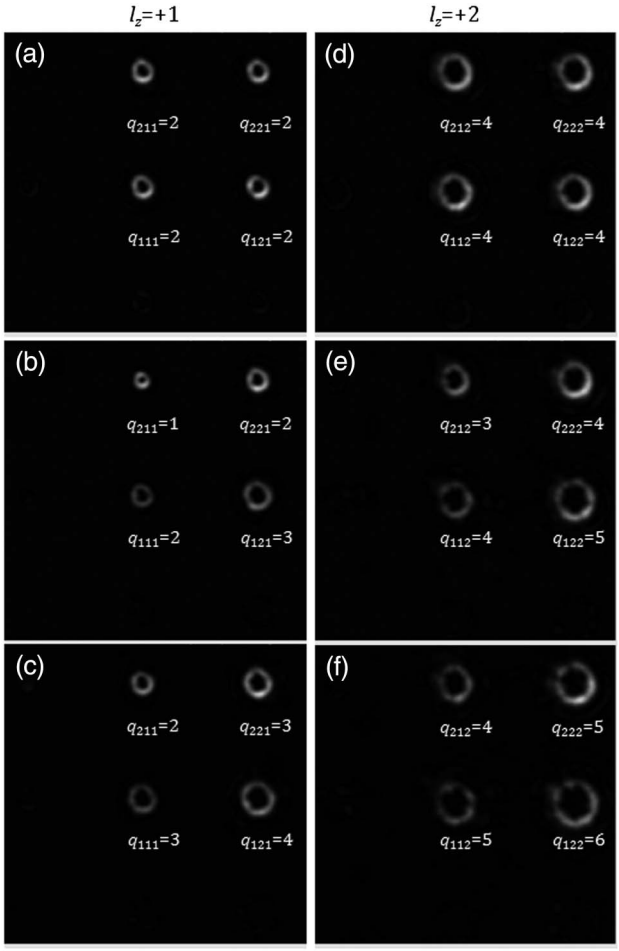

Fig. 8. Experimental diffraction patterns generated with 3D optimal phase gratings. Left and right columns show images at axial planes $l_Z = +1$ and $l_Z = +2$, respectively. (+1, +2) lens multiplied by: (a) and (d) grating with $q_Z = +2$; (b) and (e) grating with $q_X = +1$, $q_Y = -1$, and $q_Z = +2$; and (c) and (f) grating with $q_X = +1$, $q_Y = -1$, $q_Z = +2$, and $q_G = +1$. The generated charge $q_{l_X l_Y l_Z}$ is indicated at each diffraction order (l_X, l_Y, l_Z).

The first- and second-order focalizations correspond, therefore, to focal lengths $f_1 = f = -4000$ mm and $f_2 = f/2 = -2000$ mm, respectively. The experimental system keeps the glass lens used in the previous section. This way the two focusing planes appear in two close planes and the scale of the Fourier transform is very similar [13]. By applying the Gaussian lens equation, approximated distances $d_1 = 68$ cm and $d_2 = 72$ cm from the SLM are derived for the first ($l_Z = 1$) and second ($l_Z = 2$) harmonic lens terms. Note that these lens values can be easily changed to provide closer spacing between the focal planes.

In both figures, the left column corresponds always to the farther focalization in the first-order plane ($l_Z = +1$), while the right column corresponds to the closer focalization obtained with the same mask in the second-order plane ($l_Z = +2$). Let us first analyze the results in Fig. 7, where no topological charge q_z is added to the lens function. Figures 7(a) and 7(e) correspond to the on-axis focalizations when simply the lens is encoded on the SLM [i.e., like the lens shown in Fig. 6(a)]. This is obtained by applying the phase LUT only to the quadratic phase term. i.e., the pattern encoded onto the SLM is

$$\exp(i\varphi(x,y)) = \mathbf{LUT}_{12}\left[\exp\left(i\frac{\pi r^2}{\lambda f}\right)\right]. \qquad (10)$$

Two bright focalizations are obtained on axis, corresponding to the two harmonic orders $l_Z = +1$ and $l_Z = +2$ of the quadratic phase factor.

Next, we multiplied this phase mask by the optimal grating producing four diffraction orders in a plane [i.e., like the phase function shown in Fig. 6(b)]. The corresponding results shown in Figs. 7(b) and 7(f) show the diffraction pattern with the four bright spots replicated in both focusing planes.

Next an additional global topological charge $q_G = +2$ is added to the phase pattern. The results are shown in Figs. 7(c) and 7(g). Now the same vortex beam is convolved with all the previous delta functions, and, therefore, the same topological charge is replicated onto all diffraction orders in both focusing planes.

Finally, Figs. 7(d) and 7(h) correspond to multiplying the phase function in Eq. (10) by an optimal grating with charges $q_X = +1$ and $q_Y = -1$. The situation is therefore identical to that shown in Fig. 5(f), but now it is replicated on two different axial planes, $l_Z = +1$ and $l_Z = +2$, since the lens function has no additional charge. Note that, in all these cases, the DC order that is produced by the encoding method is always absent (as opposite to the cases shown in Figs. 3 and 5), since it is focused in a different plane corresponding to $l_Z = 0$.

As a final set of experiments, Fig. 8 shows different cases when we add a spiral phase term with topological charge q_Z together with the lens, in order to produce different vortex charge distribution in different focusing planes.

We start by considering the case where $q_X = q_Y = 0$, but $q_Z = +2$. This is shown in Figs. 8(a) and 8(e). In the first focalization plane [$l_Z = +1$, Fig. 8(a)], now a charge q_Z is added to all four produced diffraction orders, and they all show the same diameter. In the closer focalization plane [$l_Z = +2$, Fig. 8(e)], however, the added charge is $2q_Z$, and, therefore, the diameter is again the same for all diffraction orders in this plane, but it is larger compared with the previous case.

Next Figs. 8(b) and 8(f) correspond to the case where charges $q_X = +1$ and $q_Y = -1$ are combined with $q_Z = +2$. In the first ($l_Z = +1$) plane [Fig. 8(b)] the charges at each of the four diffraction orders are $q_{111} = q_X + q_Y + q_Z = +2$, $q_{211} = 2q_X + q_Y + q_Z = +3$, $q_{121} = q_X + 2q_Y + q_Z = +1$, and $q_{221} = 2q_X + 2q_Y + q_Z = +2$. This is why the smallest circle of light, corresponding to a charge $q = +1$, appears now at location $(p_X, p_Y) = (\gamma_X, 2\gamma_Y)$. Note now the difference with the second focusing plane ($l_Z = +2$),

shown in Fig. 8(f). In this case, the same in-plane locations show vortex beams with higher topological charge, which are now given by $q_{112} = q_X + q_Y + 2q_Z = +4$, $q_{212} = 2q_X + q_Y + 2q_Z = +5$, $q_{122} = q_X + 2q_Y + 2q_Z = +3$, and $q_{222} = 2q_X + 2q_Y + 2q_Z = +4$.

Finally, Figs. 8(c) and 8(g) show the same case, but an additional global spiral phase term with $q_G = +1$ is added. Therefore, this adds an additional $+1$ value to the charge distributions on the previous configuration. This can be noticed by comparing the results in Figs. 7(b) and 8(f), since the same vortex structure is obtained, but all circles of light show a larger diameter.

5. Conclusions

In summary, we have presented different variations for producing 3D arrays of vortex beam focalizations by properly combining linear, quadratic, and spiral phase factors with phase mapping (LUT) profiles designed to create optimal phase gratings. We probed the various vortex array distributions that can be created when the phase LUTs are applied at different stages of the diffractive mask design. Since the phase LUTs provide harmonic orders to the originally encoded blazed phase pattern, the diffraction pattern can be explained by the arithmetic combination of the harmonic orders generated in each element. Harmonic orders of blazed linear phases provide different locations within a plane, while harmonic orders of blazed quadratic phases provide focalization in different planes. Finally, harmonic orders of the blazed spiral phase provide higher topological charges. The arithmetics of these phase LUT operations can then be used to explain the 3D distribution of vortex beams.

For clarification, in this work we concentrated on designs where all of the output spots occur in the first quadrant. This design is useful to avoid the DC order originated from possible encoding errors caused by the SLM's limited spatial resolution or by possible deviations from ideal phase designs caused by limitations of the SLM phase modulation. We presented experimental results of all the cases considered, which prove the theory and find excellent agreement with theory. However, it is clear that this subject can be greatly expanded by choosing different grating LUTs and different combinations of charges for the three dimensions.

IM acknowledges financial support from the Spanish Ministerio de Economía y Competitividad and FEDER funds through project FIS2012-39158-C02-02.

References

1. S. Jeon, J.-U. Park, R. Cirelli, S. Yang, C. E. Heitzman, P. V. Braun, P. J. A. Kenis, and J. A. Rogers, "Fabricating complex three-dimensional nanostructures with high-resolution conformable phase masks," Proc. Natl. Acad. Sci. USA **101**, 12428–12433 (2004).
2. E. Schonbrun, R. Piestun, P. Jordan, J. Cooper, K. D. Wulff, J. Courtial, and M. Padgett, "3D interferometric optical tweezers using a single spatial light modulator," Opt. Express **13**, 3777–3786 (2005).
3. V. G. Shvedov, C. Hnatovsky, N. Shostka, A. V. Rode, and W. Krolikowski, "Optical manipulation of particle ensembles in air," Opt. Lett. **37**, 1934–1936 (2012).
4. D. G. Grier, "A revolution in optical manipulation," Nature **424**, 810–816 (2003).
5. S. Wong, M. Deubel, F. Pérez-Willard, S. John, G. A. Ozin, M. Wegener, and G. von Freymann, "Direct laser writing of three-dimensional photonic crystals with a complete photonic bandgap in chalcogenide glasses," Adv. Mater. **18**, 265–269 (2006).
6. T. Kondo, S. Matsuo, S. Juodkazis, and J. Misawa, "Femtosecond laser interference technique with diffractive beam splitter for fabrication of three-dimensional photonic crystals," Appl. Phys. Lett. **79**, 725–727 (2001).
7. Y. Kuroiwa, N. Takeshima, Y. Narita, S. Tanaka, and K. Hirao, "Arbitrary micropatterning method in femtosecond laser microprocessing using diffractive optical elements," Opt. Express **12**, 1908–1915 (2004).
8. J.-I. Kato, N. Takeyasu, Y. Adachi, H.-B. Sun, and S. Kawata, "Multiple-spot parallel processing for laser micronanofabrication," Appl. Phys. Lett. **86**, 044102 (2005).
9. S. Hasegawa, Y. Hayasaki, and N. Nishida, "Holographic femtosecond laser processing with multiplexed phase Fresnel lenses," Opt. Lett. **31**, 1705–1707 (2006).
10. Y. Hayasaki, T. Sugimoto, A. Takita, and N. Nishida, "Variable holographic femtosecond laser processing by use of a spatial light modulator," Appl. Phys. Lett. **87**, 031101 (2005).
11. H. Dammann and E. Klotz, "Coherent optical generation and inspection of two-dimensional periodic structures," Opt. Acta **24**, 505–515 (1977).
12. D. Prongué, H. P. Herzig, R. Dändliker, and M. T. Gale, "Optimized kinoform structures for highly efficient fan-out elements," Appl. Opt. **31**, 5706–5711 (1992).
13. J. A. Davis, I. Moreno, J. L. Martínez, T. J. Hernandez, and D. M. Cottrell, "Creating 3D lattice patterns using programmable Dammann gratings," Appl. Opt. **50**, 3653–3657 (2011).
14. J. Yu, C. Zhou, W. Jia, W. Cao, S. Wang, J. Ma, and H. Cao, "Three-dimensional Dammann array," Appl. Opt. **51**, 1619–1630 (2012).
15. V. Yu. Bazhenov, V. Vasnetsov, and M. S. Soskin, "Laser-beams with screw dislocations in their wave-fronts," JETP Lett. **52**, 429–431 (1990).
16. N. R. Heckenberg, R. McDuff, C. P. Smith, and A. G. White, "Generation of optical phase singularities by computer-generated holograms," Opt. Lett. **17**, 221–223 (1992).
17. S. H. Tao, X.-C. Yuan, J. Lin, and R. E. Burge, "Sequence of focused optical vortices generated by a spiral fractal zone plate," Appl. Phys. Lett. **89**, 031105 (2006).
18. J. Yu, C. Zhou, W. Jia, A. Hu, W. Cao, J. Wu, and S. Wang, "Three-dimensional Dammann vortex array with tunable topological charge," Appl. Opt. **51**, 2485–2490 (2012).
19. A. Calabuig, S. Sánchez-Ruiz, L. Martínez-León, E. Tajahuerce, M. Fernández-Alonso, W. D. Furlan, J. A. Monsoriu, and A. Pons-Martí, "Generation of programmable 3D optical vortex structures through devil's vortex-lens arrays," Appl. Opt. **52**, 5822–5829 (2013).
20. I. Moreno, J. A. Davis, D. M. Cottrell, N. Zhang, and X. C. Yuan, "Encoding generalized phase functions on Dammann gratings," Opt. Lett. **35**, 1536–1538 (2010).
21. J. Yu, C. Zhou, W. Jia, A. Hu, W. Cao, J. Wu, and S. Wang, "Generation of dipole vortex array using spiral Dammann zone plates," Appl. Opt. **51**, 6799–6804 (2012).
22. L. A. Romero and F. M. Dickey, "Theory of optimal beam splitting by phase gratings. I. One-dimensional gratings," J. Opt. Soc. Am. A **24**, 2280–2295 (2007).
23. L. A. Romero and F. M. Dickey, "The mathematical theory of laser beam-splitting gratings," Prog. Opt. **54**, 319–386 (2010).
24. J. Albero, I. Moreno, J. A. Davis, D. M. Cottrell, and D. Sand, "Generalized phase diffraction gratings with tailored intensity," Opt. Lett. **37**, 4227–4229 (2012).

25. J. Albero, J. A. Davis, D. M. Cottrell, C. E. Granger, K. R. McCormick, and I. Moreno, "Generalized diffractive optical elements with asymmetric harmonic response and phase control," Appl. Opt. **52**, 3637–3644 (2013).
26. http://support.microsoft.com/kb/214115.
27. J. Albero, P. García-Martínez, J. L. Martínez, and I. Moreno, "Second order diffractive optical elements in a spatial light modulator with large phase dynamic range," Opt. Lasers Eng. **51**, 111–115 (2013).
28. J. A. Davis, P. Tsai, D. M. Cottrell, T. Sonehara, and J. Amako, "Transmission variations in liquid crystal spatial light modulators caused by interference and diffraction effects," Opt. Eng. **38**, 1051–1057 (1999).
29. I. Moreno, J. A. Davis, B. M. L. Pascoguin, M. J. Mitry, and D. M. Cottrell, "Vortex sensing diffraction gratings," Opt. Lett. **34**, 2927–2929 (2009).
30. K. Crabtree, J. A. Davis, and I. Moreno, "Optical processing with vortex producing lenses," Appl. Opt. **43**, 1360–1367 (2004).